Comparison of control strategies performance for a Wave Energy Converter

Duarte Valério, Pedro Beirão, Mário J. G. C. Mendes and José Sá da Costa

Abstract— **The Archimedes Wave Swing (AWS) is a a fully-submerged Wave Energy Converter (WEC), that is to say, a device that converts the kinetic energy of sea waves into electricity. A first prototype of the AWS has already been built and tested. This paper presents simulation results of the performance of several control strategies applied to this device, including PID control, reactive control, phase and amplitude control, latching control, feedback linearisation control, internal model control, switching control, and combinations thereof. Linear, white-box nonlinear, and neural network models were employed. Significant (above threefold) increases in yearly energy production were found to be possible with properly designed control strategies.**

I. INTRODUCTION

Sea waves are a source of renewable energy. They represent an estimated power of 2 TW worldwide, and it is possible to convert part of this wave power into electricity. Several devices for this purpose, known as wave energy converters (WECs), are under development, using different working principles and designed for different types of locations. Modelling and control play an important role in improving the efficiency achieved.

This paper addresses a particular WEC, the first prototype of the Archimedes Wave Swing (AWS). It sums up simulation results, obtained with different identification and control techniques, already published elsewhere, comparing their relative performances.

II. THE ARCHIMEDES WAVE SWING

The first-generation AWS is an off-shore submerged WEC, with a diameter neglectable when compared to a typical wave length (thus termed a point absorber), consisting in two main cylindrical and hollow parts, the floater and the silo, mounted in a structure to keep them together, with air trapped within floater and silo. The silo is fixed to the structure and thereby to the sea-bottom; the floater is free to heave up and down, within the range of mechanical end-stops. The working principle is simple: when a wave crest passes over the AWS, the height of water increases, so does the pressure compressing the air within, and the floater moves down; when a wave trough passes over the AWS, the height of water decreases, so does the pressure, the air expands and the floater moves up. (This is depicted in Fig. 1.) The heaving motion of the floater is converted into electricity by an electrical linear generator (ELG). Water dampers are mounted in the AWS structure, outside silo and floater, and become active when the floater gets close to the mechanical end-stops, providing an additional damping force, to prevent any strong collision.

A prototype of the AWS has already been built and tested in Portugal, near Leixões, 5 km away from the coast, where it was 43 m under water. After the tests in 2004, this prototype was decommissioned. A second-generation, improved prototype is currently under development.

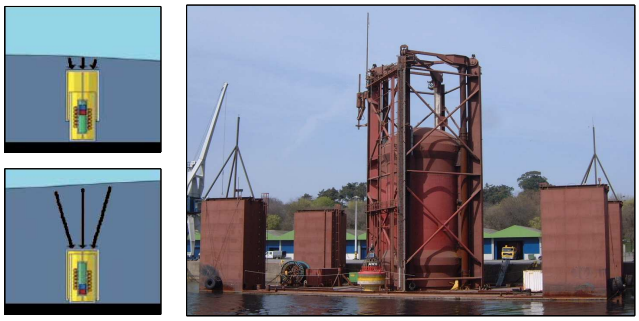

Fig. 1. The AWS working principle and the first prototype before submersion

A. Wave models

The wave climate of the test site may be statistically characterised with data from the ONDATLAS software [1]. The location available nearer to the test site is Leixões–buoy, $41°12.2'$ N, $9°5.3'$ W. Table I gives for this location average significant values of the wave height H_s (from trough to crest) and maximum and minimum values of the wave energy period T_e. In this paper simulations are performed using regular and irregular waves. The first are sinusoidal, with values for amplitude and period congruent with Table I. For the latter, thirteen waves were used, one for each month of the year and one for the whole year data. These irregular waves were generated using Pierson-Moskowitz's spectrum [2], that models the behaviour of

Authors would like to thank AWS Ocean Energy Ltd. Both Pedro Beirão and Mário J. G. C. Mendes were partially supported by the "Programa do FSE-UE, PRODEP III, acção 5.3, III QCA". Duarte Valério was partially supported by grant SFRH/BPD/20636/2004 of FCT, funded by POCI 2010, POS C, FSE and MCTES. Research for this paper was partially supported by grant PTDC/EME-CRO/70341/2006 of FCT, funded by POCI 2010, POS C, FSE and MCTES; and by the Portuguese Government and FEDER under program "Programa de Financiamento Plurianual das Unidades de I&D da FCT" (POCTI-SFA-10-46-IDMEC).

D. Valério and J. Sá da Costa are with IDMEC/IST, TULisbon, Av. Rovisco Pais 1, 1049-001 Lisboa, Portugal. {dvalerio,sadacosta}@dem.ist.utl.pt

P. Beirão is with Instituto Superior de Engenharia de Coimbra, Dept. Mechanical Engineering, R. Pedro Nunes, 3030-199 Coimbra, Portugal. pbeirao@isec.pt

M. J. G. C. Mendes is with IDMEC / ISEL, Instituto Superior de Engenharia de Lisboa, R. Conselheiro Emídio Navarro, 1, 1959-007 Lisboa, Portugal. mmendes@dem.isel.ipl.pt

North-Atlantic sea waves, and is given by

$$\mathcal{S}(\omega) = \frac{A}{\omega^5}\ \exp\left(-\frac{B}{\omega^4}\right) \tag{1}$$

Here, the wave energy spectrum $\mathcal{S}$ is a function such that $\int_0^{+\infty} \mathcal{S}(\omega)d\omega$ is the mean-square value of the wave elevation (equal to one half of H_s). The numerical values $A = 0.780$ (SI) and $B = 3.11/H_s^2$ were used. Values for H_s and for T_e (from which the limits of the frequency range were then found) were provided by Table I. There are significant variations in wave characteristics along the year, and it is useful to divide months according to the average energy content of waves, that depends on H_s. In what follows, "summer" refers to those months when H_s is above average (the May–September period), and "winter" to the rest of the year.

B. Nonlinear model of the AWS

Applying Newton's law to the floater, we get

$$f_{pi} - f_{hs} - f_{rad} + f_{exc} - w_f - f_n - f_v - f_m - f_{wd} - f_{lg} = m\ddot{\xi} \tag{2}$$

The floater's mass is m and its vertical acceleration is $\ddot{\xi}$. The force acting thereupon is the sum of the forces due to internal air pressure f_{pi}, to the hydrostatic impulse f_{hs}, to wave radiation f_{rad} (this being the force exerted on the AWS by the wave that the floater creates by its movement), to wave excitation f_{exc} (this being the force exerted on the AWS by the incident sea waves assuming that the floater is not moving), to the weight of the floater w_f, to a nitrogen cylinder extant inside the AWS f_n, to the hydrodynamic viscous drag f_v, to mechanical friction f_m, to the water dampers f_{wd}, and to the ELG f_{lg}. The last two are the forces we can control, and their sum will be called control force f_u. Since the water dampers are only sporadically used, most of the time $f_u = f_{lg} + f_{exc} \approx f_{lg}$ (though not when the floater gets close to the end-stops). In (2), positive values are given to the most natural direction; hence most forces point downwards. Small-case letters are being used for variables in the time-domain; their Laplace transforms (in the frequency domain) will be denoted using the corresponding capitals. (Hence $\Xi(s) \stackrel{\text{def}}{=} \mathcal{L}[\xi(t)]$, $F_{lg}(s) \stackrel{\text{def}}{=} \mathcal{L}[f_{lg}(t)]$, and so on.)

The expressions of most forces in (2) are nonlinear; they are given in [3], [4]. They were implemented in a Simulink-based simulator of the AWS, the AWS Time-Domain Model (TDM), that was used for the simulations presented in this paper[1]. Data provided by this nonlinear model was also used to identify the other models in this section, because extant data from the prototype is scant and insufficient.

[1]When preparing this paper, several parameters and significant values of the model have been altered, due to industrial protection reasons. Thus results below should not be construed as indicative of the AWS first prototype actual performance. Nevertheless, they are significant as they reveal the efficacy of control strategies, and are deemed useful for the development of the second-generation prototype.

C. Linear model of the AWS

In spite of the significant nonlinearities present, from the description above the AWS can be expected to behave like a mass–spring–damper system. Applying Levy's identification method [5] to AWS simulation outputs, a second-order linear approximate model is found [6], [7]:

$$\frac{\Xi(s)}{F_{exc}(s) + F_{lg}(s)} = \frac{2.259 \times 10^{-6}}{0.6324s^2 + 0.1733s + 1} \tag{3}$$

It is usual [2] to define an impedance $Z_i(\omega)$ given by

$$\frac{1}{Z_i(s)} = \frac{\dot{\Xi}(s)}{F_{exc}(s) + F_{lg}(s)} \Leftrightarrow Z_i(s) = \frac{S + Rs + ms^2}{s} \tag{4}$$

Comparing (3) with (4) it is seen that $m = 2.7995 \times 10^5$, $R = 7.6715 \times 10^4$ and $S = 4.4267 \times 10^5$.

D. Neural network models of the AWS

Artificial NNs appeared as an attempt to find mathematical models of how the human nervous system works. They were found to be too simple for that, but they proved able to model nonlinear plants, static or dynamic. Algorithms were developed to adjust (or train) the parameters of a NN according to a given collection of input-output data. Thus a black-box model is found. The basics of NNs fall outside the scope of this paper; see for instance [8] and other references below.

Among possible architectures for dynamic NNs [8], [9], it has been found [10] that the best for the AWS is the one known as locally recurrent network (LRN) models, using neurons arranged in two layers (the hidden layer and the output layer). NN inputs are fed to the hidden layer; this layer's outputs are fed to the output layer, and are also delayed and fed back as NN inputs (known as context units). The output layer's outputs are the NN's outputs. Fig. 2 shows a LRN; x is the NN's input (here a 2-element vector), $\hat{y}$ is the NN's output (here as a 1-element vector), N_h is the number of neurons in the hidden layer, and c denotes the context units. LRNs with only two layers, using activation functions $f(\zeta) = \tanh(\zeta)$ in the hidden layer and $f(\zeta) = \zeta$ in the output layer are called Elman NNs [11]. For AWS LRN models the activation function $f(\zeta) = \text{logsig}(\zeta) = \frac{1}{1+e^{-\zeta}}$ was also used.

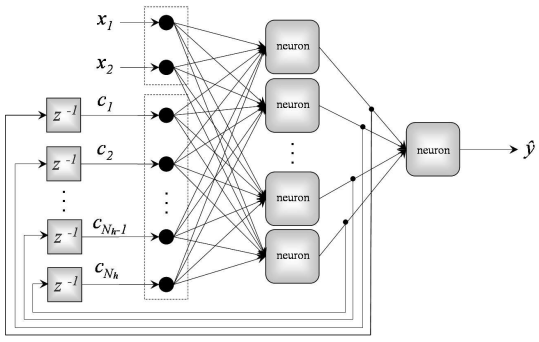

Fig. 2. Scheme of an Elman dynamic neural network

TABLE I

CHARACTERISTICS OF SEVERAL IRREGULAR WAVES ACCORDING TO ONDATLAS

	Jan	Feb	Mar	Apr	May	Jun	Jul	Aug	Sep	Oct	Nov	Dec	Whole year
H_s / m	3.2	3.0	2.6	2.5	1.8	1.7	1.5	1.6	1.9	2.3	2.8	3.1	2.3
$T_{e,min}$ / s	5.8	5.8	5.2	5.5	5.0	4.7	4.6	5.0	5.2	5.3	5.5	5.3	4.6
$T_{e,max}$ / s	16.1	14.5	13.7	14.8	12.2	9.7	11.1	10.5	12.0	12.6	13.3	14.2	16.1

The backpropagation algorithm, together with Levenberg-Marquardt optimisation [12], was used as the NN training algorithm. Its performance depends heavily on the training data. The data should reflect all possible working conditions of the system. Too few data may be less than enough to train the NN properly. Too much data may overtrain it, so that it will just reproduce the training set and be unable to give meaningful outputs for new situations. It may also exhaust available memory, and cause numerical problems.

Direct and inverse NN models of the AWS were built using Matlab's Neural Network Toolbox. In such cases it may be useful to reuse input structures from existing linear models [8]. So the wave excitation force f_{exc} and the force exerted by the ELG f_{lg} were selected as inputs, and the floater's vertical velocity $\dot{\xi}$ as output. For the AWS inverse model, the inputs were f_{exc} and $\dot{\xi}$, and the output f_{lg}. Strictly speaking, the inverse model obtained is a partial inverse model, because f_{exc} is always considered an input (because it is not created by the AWS; it is better viewed as a perturbation).

A 600 s wave corresponding to the parameters of the whole year was fed to the AWS TDM; the values of f_{exc}, f_{lg} and $\dot{\xi}$ obtained were used to train the NNs (see details in [10]). After some trial and error (sometimes necessary in similar cases), the NNs with the characteristics given in Table II were chosen. Direct models are denoted with a D and inverse models with a I. Models D1 and I1 have a good performance all over the year; models D2 and I2 (the latter equal to I1) achieve better results during winter; models D3 and I3 achieve better results during summer.

III. CONTROL STRATEGIES

A. The original AWS controller

If the floater is left heaving freely, the ELG still exerts a residual force, from which some electricity is produced. This situation without any control is clearly undesirable. Thus a controller was provided for the AWS prototype, exerting a control force f_u given by

$$|f_u| = \left|\dot{\xi}\right| k_p \left|\dot{\xi} - \dot{\xi}_{stpl}\right| \tag{5}$$

$$\left|\dot{\xi}_{stpl}\right| = \begin{cases} \frac{2\pi}{10} 3.5 \sqrt{1 - \left(\frac{\xi}{3.5}\right)^2} & \text{if } |\xi| < 3.5 \text{ m} \\ 0 & \text{if } |\xi| \geq 3.5 \text{ m} \end{cases} \tag{6}$$

In (5), $\dot{\xi}_{stpl}$ is a reference value for $\dot{\xi}$, and k_p is the gain of a proportional controller, given by $k_p = 5 \times 10^6$. Constant 3.5 m shows up in (6) because it is the position of the floater's end-stops. Constant 10 s shows up because it is a reasonable value for the period of an incoming wave.

B. Reactive control

It is possible to show [2] that a WEC with a dynamic behaviour described exactly by a second-order transfer function without zeros will maximise energy absorption if

$$\frac{F_u(\omega)}{\dot{\Xi}(\omega)} = -Z_i^*(\omega) \tag{7}$$

where * denotes the complex conjugate. This is called *reactive control* and was implemented with the AWS TDM replacing the noncausal transfer function $-Z_i^*(s)$ with $\frac{-Z_i^*(s)}{s+1}$, the extra pole placed at -1 ensuring causality. Several locations have been tested for the pole, and the one leading to a larger absorption of wave energy was kept. An alternative procedure would have been to identify from the frequency response of $-Z_i^*$ a causal, stable, approximate transfer function with a similar response in the frequency range of interest; this approach was pursued, but led to no acceptable results [7], [13].

C. Phase and amplitude control

It is also possible to show that when (7) is satisfied $\dot{\xi}$ is in phase with f_{exc}. An optimum value for the proportionality constant can also be found. The enforcement of these two conditions by a suitable controller is called *phase and amplitude control*. For the AWS TDM a proportional controller was used, obtained maximising the absorbed wave energy with MatLab function `fminsearch` (simplex direct search method), the optimum being 5.1348×10^4. Integral and derivative terms (forming a PID controller) did not improve results. Internal model control was also used, as seen below in subsection III-D. Since the AWS is nonlinear and (3) is just an approximation, phase and amplitude control is not necessarily optimum [7], [13]. Indeed simulations have shown that modifying the proportionality constant leads to a higher energy production. The resulting set-point is given by

$$\dot{\xi}_{stp2} = \frac{2.2}{\max |f_{exc}|} f_{exc} \tag{8}$$

Constant 2.2 appears because the nominal value for the floater's vertical velocity that the AWS should work with is 2.2 m/s [14].

D. Internal Model Control

The *internal model control* (IMC) methodology [15] mentioned above makes use of the control scheme of Fig. 3. In that control loop, G is the plant to control, G' is a model of G, G^* is an inverse of G' (or at least a plant as close as possible to the inverse of G'), and F is some judiciously chosen filter. If G' were exact, G^* were the exact inverse of G' (and hence also of G), and F were

TABLE II

LINEAR AND NEURAL NETWORK MODELS OF THE AWS

	(3)	D1	I1	D2	I2	D3	I3
Inputs	$f_{exc} + f_{lg}$	f_{exc}, f_{lg}	f_{exc}, $\dot{\xi}$	f_{exc}, f_{lg}	f_{exc}, $\dot{\xi}$	f_{exc}, f_{lg}	f_{exc}, $\dot{\xi}$
Outputs	$\dot{\xi}$	$\dot{\xi}$	f_{lg}	$\dot{\xi}$	f_{lg}	$\dot{\xi}$	f_{lg}
Type	Linear, direct	Elman NN, direct	Elman NN, inverse	Elman NN, direct	Elman NN, inverse	LRN, direct	LRN, inverse
Hidden layer	—	8 neurons	10 neurons	10 neurons	10 neurons	20 neurons	10 neurons
Activation	—	tanh	tanh	tanh	tanh	logsig	tanh
functions	—	linear	linear	linear	linear	logsig	logsig
Training	—	7 epochs	5 epochs	3 epochs	5 epochs	8 epochs	4 epochs

unity, control would be perfect. Since no models are perfect, the error will not be exactly the disturbance. That is also why F exists and is usually a low-pass filter: to reduce the influence of high-frequency modelling errors. It also helps ensuring that product FG^* is realisable. The AWS TDM was controlled with IMC using reference (8) and employing two types of models: linear models and NN models. The NN models employed were D1 and I1 [10], [16]. When linear models were used [17], G' was (3) multiplied by s (this additional zero at the origin serving to have the floater's vertical velocity—and not its position—as the output), and $G^* = \frac{1}{G'}$. Since G^* is not causal, the filter F had to have more poles than zeros. It was found by trial and error that a second-order filter without zeros was the best option. The position of the poles was adjusted so as to maximise the absorbed wave energy for the simulation that uses an irregular wave with parameters corresponding to the month of March (deemed to be a significant month). The values found were

$$F = \frac{600}{(s+23)(s+20)} \tag{9}$$

This is reasonable since it corresponds to a low-pass filter that preserves the frequencies where waves are expected to appear, while cutting off higher ones. Because of this, the product FG^* has an integral action. Since the signal it acts upon (labelled e in Fig. 3) has a residual non-null average, this lead to an ever-increasing (or ever-decreasing) control action, something that was not intended. To prevent this, the control action had to be corrected, by subtracting its average, computed from the beginning of the simulation and actualised on-line.

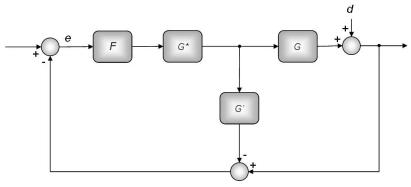

Fig. 3. Block diagram for Internal Model Control

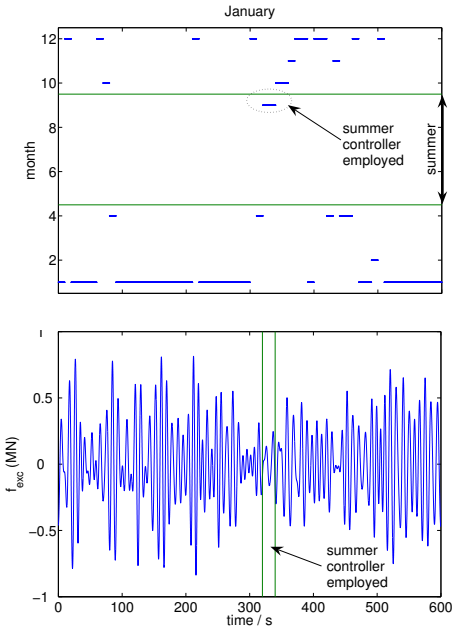

Fig. 4. Example of months detected

E. Switching control

During summer, when waves have less energy, IMC with NN models D1 and I1 performs poorly when compared with winter. This can be improved *switching control* between different controllers [18] according to whether waves are more or less energetic. For that purpose two IMC controllers were implemented, one with models D2 and I2 and one with models D3 and I3 [16]. NN models are expected to cope with nonlinearities, but it is not surprising that different models should perform better for rather different inputs. The use of three different controllers was attempted, but was not profitable, as this resulted in no significant improvement in performance.

To know which controller is to be used in each instant, the power density spectrum of the wave, calculated from the previous 100 s of simulation, is obtained and compared to those typical of each month. This is done every 10 s, so that no controller ever works for less time; this option was taken lest switching more often should lead to instability problems, and also because the computation of the spectrum takes some time and it would not do to perform it every 0.02 s. (During the first 10 s, January is assumed as output by default.) Since every wave, whatever the month, has more calm and more agitated periods, the month identified will often be incorrect; but this poses no problem, since all that is intended is to distinguish between summer and winter; that sometimes, when the wave is unusually calm or unusually agitated, a different controller is used, is not cause of concern, since this may even help improve the performance. Fig. 4 shows the month detected when a wave typical for January is employed.

The month identified is often correct, but clearly not always; yet the summer controller is only used during a 20 s period during which, as the evolution of f_{exc} shows, the wave amplitude is small and the period high.

F. Feedback linearisation

Feedback linearisation is a control strategy which aims to provide a control action judiciously chosen to cancel the nonlinear dynamics of the plant, so that the closed-loop dynamics will be (as much as possible) linear [19]. We assume that the ELG and the water dampers, which are to generate f_u, can respond immediately and without restrictions. This is really not the case (both devices saturate and have internal dynamics), but is an assumption good enough for our purposes. Hence

$$\begin{aligned} -f_u &= m\ddot{\xi} - f_{pi} + f_{hs} + \\ &\quad + f_{rad} - f_{exc} + f_n + f_v + f_m + w_f \end{aligned} \tag{10}$$

Let us provide a control action given by

$$\begin{aligned} f_u &= f_{pi} - f_{hs} - f_{rad} - f_n - f_v - f_m - \\ &\quad - w_f - m\ddot{\Xi} + \dot{\Xi}\frac{\max|f_{exc}|}{2.2} \end{aligned} \tag{11}$$

This is possible because there are explicit (nonlinear) expressions for all the forces involved in the right-hand side of (11). We will end up with a dynamic behaviour equal to (8) [20], [7].

G. Latching control

To have the floater's velocity in phase with the wave excitation force, *latching control* latches the floater when its velocity vanishes, and then releases it when it is predicted that its maximum (or minimum) velocity will coincide (in time) with the maximum (or minimum) of the wave excitation force. This is a highly nonlinear control strategy, that does not employ an amplitude setpoint for velocity. An ideal depiction of latching control is shown in Fig. 5. The floater of the AWS can be latched using both the ELG and the water dampers. The algorithm implemented was as follows [7]. When the floater is latched, the duration of the last unlatched period is obtained. The next unlatched period is assumed to be going to last the same as the previous one. The floater's velocity is assumed to have its maximum (or minimum) precisely at the centre of that time interval. So the latching time is reckoned for that velocity maximum (or minimum) to coincide in time with the next maximum (or minimum) of the wave excitation force. The force required to latch the floater depends on the amplitude and period of the incoming wave, larger waves requiring a larger force and smaller waves requiring a smaller force. The forces for each wave amplitude and period are those necessary to latch effectively the floater when the incident wave is regular and has the required amplitude and period; suitable values were obtained beforehand with the AWS TDM for some regular waves, and then interpolated and extrapolated as needed.

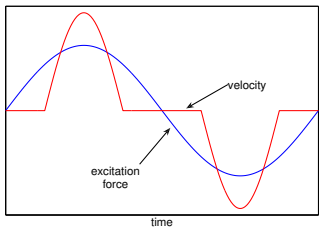

Fig. 5. Ideal evolution of the excitation force and of the floater's velocity with latching control

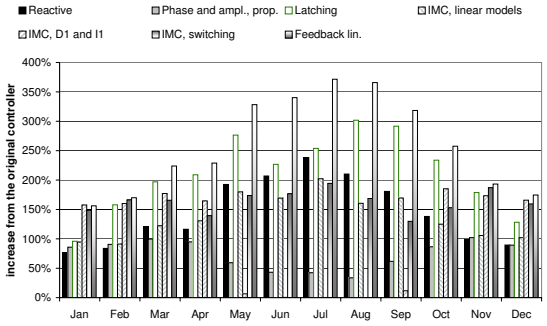

Fig. 6. Results from Table III plotted

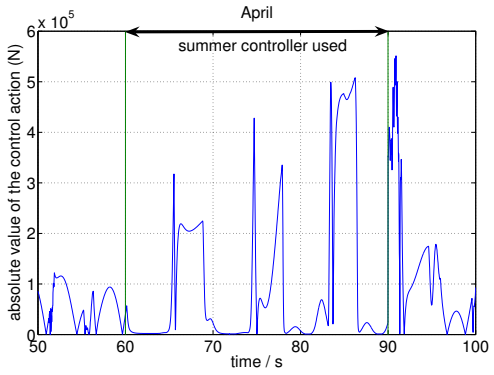

Fig. 7. Evolution of the control action when controllers are switched (figurative data)

IV. RESULTS AND COMMENTS

Power extraction values for simulation results of all the control strategies above are given in Table III and represented in Fig. 6. Increases are reckoned against the performance of the original controller. These results call for the following comments.

Control strategies are given in Table III by increasing order of performance. The most striking result is that the best performing one leads to an energy production over three times larger than that of the worst performing one. This shows how important the optimisation of a control algorithm is for a WEC.

NN models are stable, and so are each the IMC control loops considered separately; switching controllers, however, might lead to abrupt changes in the control action, possibly leading to instability. This, however, is not the case; Fig. 7 (taken from a simulation with a wave typical for April) shows

TABLE III

POWER IN kW OBTAINED UNDER SEVERAL IRREGULAR WAVES (FIGURATIVE DATA)

	Jan	Feb	Mar	Apr	May	Jun	Jul	Aug	Sep	Oct	Nov	Dec	Whole year
Original controller	44.9	35.6	22.7	21.0	6.5	4.6	3.2	3.9	7.8	14.9	27.9	38.8	19.2
phase & ampl. control with P controller	83.5	67.9	45.4	40.8	10.3	6.6	4.5	5.2	12.6	27.8	56.3	73.4	36.2
% increase	86	91	100	95	59	43	42	34	62	86	102	89	87
Reactive control	79.1	65.5	50.1	45.3	18.9	14.2	10.8	12.2	21.8	35.5	55.4	73.5	40.2
% increase	76	84	120	116	193	207	238	210	181	138	99	90	108
IMC with linear model	87.5	68.1	50.6	48.3	18.1	12.5	9.6	10.2	21.0	33.5	57.4	78.3	41.3
% increase	95	91	122	131	180	169	202	160	169	125	106	102	114
IMC with NN models D1 and I1	115.7	92.6	63.0	55.4	6.9	4.7	3.2	3.9	8.7	42.5	76.2	103.1	47.8
% increase	158	160	177	165	6	0	0	0	12	185	173	166	148
IMC switching between NN models	111.7	94.8	60.4	50.2	17.7	12.8	9.4	10.5	17.9	37.6	80.0	100.6	50.1
% increase	149	166	166	139	174	177	194	169	130	153	187	159	160
latching control	88.1	91.9	67.5	64.7	24.4	15.1	11.3	15.8	30.5	49.7	77.7	88.5	52.1
% increase	96	158	197	209	277	227	254	302	292	234	179	128	170
feedback linearisation	115.1	96.2	73.6	68.9	27.7	20.4	15.0	18.3	32.6	53.2	81.8	106.4	59.1
% increase	156	170	224	229	328	340	371	366	318	258	193	175	206

two transitions, wherefrom no control actions arise harsher than those taking place without switching, and this is always the case. Thus it was not necessary to increase the number of controllers, to employ a filter (smoothing down the transition of control actions during a suitable period of time), or take any other measure (see for instance [21]). This is also likely because of the significant inertia of the moving parts of the AWS, and to its low-pass filter behaviour, as can be seen from linear model (3).

Better models mean better performing control strategies. Control strategies using NN models perform better than those using linear ones, and the best performing strategy (feedback linearisation) uses knowledge of the nonlinear behaviour of the plant.

All controllers based upon phase and amplitude control require knowing in advance the excitation force, and so do strategies for latching, switching and linearisation as well. In simulation this is simple; in practice, this must be predicted from measurements performed by a buoy (or buoys) judiciously placed near the AWS. Poor predictions will cause worst control performances.

All control strategies are liable to have poorer performances when implemented in a prototype (rather than simulated as above); in particular, feedback linearisation is most prone to deteriorate its achievements, because, in practice, nonlinear forces will never be so accurately cancelled as in simulations (from that point of view, controllers based upon NN models will be in advantage, since NN training is to be based upon experimental data). This means that the final choice of the control strategy always ought to take into account experimental results of controller performance.

These strategies may also be employed in other similar WECs.

REFERENCES

[1] M. T. Pontes, R. Aguiar, and H. Oliveira Pires, "A nearshore wave energy atlas for Portugal," *Journal of Offshore Mechanics and Arctic Engineering*, vol. 127, pp. 249–255, August 2005.

[2] J. Falnes, *Ocean waves and oscillating systems*. Cambridge: Cambridge University Press, 2002.

[3] J. Sá da Costa, P. Pinto, A. Sarmento, and F. Gardner, "Modelling and simulation of AWS: a wave energy extractor," in *Proceedings of the 4th IMACS Symposium on Mathematical Modelling*. Vienna: Agersin-Verlag, 2003, pp. 161–170.

[4] J. Sá da Costa, A. Sarmento, F. Gardner, P. Beirão, and A. Brito-Melo, "Time domain model of the Archimedes Wave Swing wave energy converter," in *Proceedings of the 6th European Wave and Tidal Energy Conference*, Glasgow, 2005, pp. 91–97.

[5] D. Valério, M. D. Ortigueira, and J. Sá da Costa, "Identifying a transfer function from a frequency response," *Journal of Computational and Nonlinear Dynamics*, 2008, publication scheduled for April.

[6] P. Beirão, D. Valério, and J. Sá da Costa, "Linear model identification of the Archimedes Wave Swing," in *IEEE International Conference on Power Engineering, Energy and Electrical Drives*, Setúbal, 2007.

[7] D. Valério, P. Beirão, and J. Sá da Costa, "Optimisation of wave energy extraction with the Archimedes Wave Swing," *Ocean Engineering*, vol. 34, no. 17-18, pp. 2330–2344, 2007.

[8] M. Nørgaard, O. Ravn, N. K. Poulsen, and L. K. Hansen, *Neural networks for modelling and control of dynamic systems: a practitioner's handbook*. London: Springer-Verlag, 2003.

[9] S. Haykin, *Neural Networks—A Comprehensive Foundation*, 2nd ed. New Jersey, U.S.A.: Prentice Hall International, Inc, 1999.

[10] P. Beirão, M. J. G. C. Mendes, D. Valério, and J. Sá da Costa, "Control of the Archimedes Wave Swing using Neural Networks," in *7th European Wave and Tidal Energy Conference*, Porto, 2007.

[11] J. Elman, "Finding structure in time," *Cognitive Science*, vol. 14, pp. 179–211, 1990.

[12] D. Marquardt, "An algorithm for least squares estimation of nonlinear parameters," *SIAM Journal on Applied Mathematics*, vol. 11, pp. 431–441, 1963.

[13] D. Valério, P. Beirão, and J. Sá da Costa, "Reactive control and phase and amplitude control applied to the Archimedes Wave Swing," in *17th International Offshore (Ocean) and Polar Engineering Conference & Exhibition*, Lisbon, 2007.

[14] H. Polinder, M. Damen, and F. Gardner, "Linear PM generator system for wave energy conversion in the AWS," *IEEE Transactions on Energy Conversion*, vol. 19, no. 3, pp. 583–589, September 2004.

[15] T. Hägglund and K. Åström, "Automatic tuning of PID controllers," in *The control handbook*, W. S. Levine, Ed. Boca Raton: CRC Press, 1996, pp. 817–826.

[16] D. Valério, M. J. G. C. Mendes, P. Beirão, and J. Sá da Costa, "Identification and control of the AWS using neural network models," *Applied Ocean Research*, 2008, submitted.

[17] J. Sá da Costa, P. Beirão, and D. Valério, "Internal Model Control applied to the Archimedes Wave Swing," in *International Conference on Control Systems and Computer Science*, Bucharest, 2007.

[18] D. Liberzon, *Switching in Systems and Control*. Boston: Birkhäuser, 2003.

[19] J. Slotine and W. Li, *Applied Nonlinear Control*. Englewood Cliffs: Prentice Hall, 1991.

[20] D. Valério, P. Beirão, and J. Sá da Costa, "Feedback linearisation control applied to the Archimedes Wave Swing," in *15th IEEE Mediterranean Conference on Control and Automation*, Athens, 2007.

[21] J. P. Hespanha and A. S. Morse, "Switching between stabilizing controllers," *Automatica*, vol. 38, pp. 1905–1917, 2002.